Geological Quarterly, 2019, **63** (3): 522–538
DOI: http://dx.doi.org/10.7306/gq.1484

Geochemistry of surface sediments from the northwestern Gulf of Mexico: implications for provenance and heavy metal contamination

John S. ARMSTRONG-ALTRIN[1, *], Alfonso V. BOTELLO[1], Susana F. VILLANUEVA[1] and Luis A. SOTO[1]

[1] Universidad Nacional Autónoma de México, Instituto de Ciencias del Mar y Limnología, Unidad de Procesos Oceánicos y Costeros, Circuito Exterior s/n, 04510 CDMX., México

Armstrong-Altrin, J.S., Botello, A.V., Villanueva, S.F., Soto, L.A., 2019. Geochemistry of surface sediments from the northwestern Gulf of Mexico: implications for provenance and heavy metal contamination. Geological Quarterly, **63** (3): 522–538 doi: 10.7306/gq.1484

Associate Editor – Wojciech Granoszewski

Thirty-five near-surface sediment samples were recovered from the continental shelf and upper slope regions of the northwestern (NW) Gulf of Mexico. The geochemical data of the sediments recovered were examined to investigate the weathering intensity, provenance, palaeo-oxygenation condition, and level of heavy metal contamination. The sediments analysed showed a moderate to high intensity of chemical weathering. Major and trace element concentrations indicated a terrigenous origin, closely related to the weathering of rocks rich in aluminosilicates. The results of this study further revealed that major rivers, the Bravo and Soto La Marina, played an important role in delivering sediments to the study area. The concentration of transition trace elements such as Cr, Cu, Ni, and V revealed that the sediments were derived from intermediate rocks such as andesite. The V/Cr, Ni/Co, and Cu/Zn ratios in the sediments were <2, <5, and <1, respectively, suggesting a depositional process occurred under well-oxygenated conditions. Principle Component Analysis (PCA) did not show a significant difference in sediment texture between the continental shelf and slope areas. The enrichment factor (EF) and Geo-accumulation index (I_{geo}) values were <2 and <1, respectively, suggesting the absence of an anthropogenic input.

Key words: Tamaulipas, deep-sea sediments, enrichment factor, contamination, principle component analysis.

INTRODUCTION

The chemical composition of detrital sediments is commonly used as a sensitive indicator of provenance (Verma and Armstrong-Altrin, 2013, 2016; Basu, 2017; Tzifas et al., 2019), to identify weathering conditions (Gabrielli et al., 2010; Xie and Chi, 2016; Ndjigui et al., 2019), and in several cases as a tool to infer heavy metal contamination (Ramos-Vázquez et al., 2017; Ma et al., 2019; Prabakaran et al., 2019). This is because sediment compositions are mostly influenced by the nature of the sedimentary processes within the depositional basin and kind of dispersal path that links provenance to the basin (Lin et al., 2014; Hou et al., 2017; Pandey and Parcha, 2017; Hernández-Hinojosa et al., 2018; Spalletti et al., 2019).

Trace elements such as Y, Cr, Th, Zr, Hf, Nb, and Ti are best suited for provenance determination, because of their relatively low mobility during sedimentary processes (Cullers, 2000). These elements occur preferentially in resistant minerals and are not released during weathering and transportation, and thus might best reflect the signature of the parent materials (McLennan et al., 1993). Therefore, they are expected to be more useful than major elements in discriminating source rock compositions (Armstrong-Altrin et al., 2004, 2013, 2015a, b; Qiu et al., 2014; Zaid, 2013, 2017; Etemad-Saeed et al., 2015; Verma et al., 2016; Ma et al., 2017; Chaudhuri et al., 2018). Similarly, the distribution of immobile elements, such as La and Th (enriched in silicic rocks) and Cr and Co (enriched in basic rocks relative to silicic rocks), have been used to infer the relative contribution of felsic and mafic sources in sediments from different sedimentary environments (Cullers et al., 1988; Madhavaraju and Lee, 2010; Madhavaraju, 2015; Ramachandran et al., 2016; Basu, 2017; Armstrong-Altrin et al., 2017; Madhavaraju et al., 2018; Velmurugan et al., 2019).

The Gulf of Mexico is a region that boasts oil reservoirs of commercial importance, and there are records of several large-scale oil spills in the area (Botello et al., 2015). The "Ixtoc I" well spill was the first to take place in the SW Gulf of Mexico, and it continued for roughly nine months. A volume of ~ 475,000 metric tons of crude oil was released into the sea. The northern Gulf of Mexico recently underwent the greatest disaster in oceanic oil spill history, i.e., the collapse of the Deepwater Horizon platform, the property of British Petroleum (BP) in April 2010, 4.9 million barrels of oil were spilled within three months (Zhang et al., 2018).

* Corresponding author, e-mail: armstrong@cmarl.unam.mx; john_arms@yahoo.com

Received: August 11, 2018; accepted: May 29, 2019; first published online: September 27, 2019

Few studies have investigated the provenance of coastal sediments, based on textural and geochemical characteristics, along the northern Gulf of Mexico (Kasper-Zubillaga et al., 2013; Armstrong-Altrin and Natalhy-Pineda., 2014; Armstrong-Altrin et al., 2015b; Hernández-Hinojosa et al., 2018). Kasper-Zubillaga et al. (2013) studied the geochemistry of beach sands from the northern part of the Gulf of Mexico and suggested that they may be used to identify the depositional environment of the sedimentary basin. Armstrong-Altrin and Natalhy-Pineda (2014) inferred the provenance based on surface microtextures on quartz grains from three beach areas in the Gulf of Mexico. Hernández-Hinojosa et al. (2018) addressed the textural and geochemical characteristics of beach sands along the western Gulf of Mexico. Tapia-Fernandez et al. (2017) studied the chemistry and U-Pb geochronology of detrital zircons in the Brujas beach and revealed the importance of rivers in contributing sediments to the Southwestern Gulf of Mexico. Recently, Armstrong-Altrin (2015) and Armstrong-Altrin and Machain-Castillo (2016) discussed the provenance of continental slope sediments from the southwestern Gulf of Mexico. Similarly, the heavy metal concentrations of the estuary sediments from the Gulf of Mexico have been documented by Botello et al. (2015) and Rosales-Hoz et al. (2015). However, provenance studies based on sediment geochemistry in the NW Gulf of Mexico are limited.

This article discusses the geochemistry of surface sediments recovered from the NW part of the Gulf of Mexico. It provides information on weathering intensity, sedimentary provenance, palaeo-oxygenation conditions and quantifies the level of heavy metal contamination in the sediments.

STUDY AREA

The study area extends along the NW Gulf of Mexico between 25°32'74.33"N–95°44'33.83"W and 22°32'81.83"N–97°56'94.17" W, including shelf and upper slope regions from 48 to 2329 m depth (Fig. 1). This sector of the Gulf of Mexico is strongly influenced by the cyclone and anticyclone gyres derived from the Loop Current. The surface oceanic circulation is predominantly towards the north, while these cyclonic processes are absent in the NW part of the Gulf of Mexico. The salinity and vertical density profiles obtained during the winter season indicated the intrusion of cold and diluted water originated from the Louisiana-Texas continental shelf (Monreal-Gómez and Salas de León, 1990; Salas de Salas-de-Leon et al., 1992). The depositional conditions on the shelf are profoundly influenced by the river runoff of three main rivers, namely the Bravo, Soto La Marina, and Panuco, and by the exporting capacity of two major coastal lagoons, namely the Madre and Tamiahua (Fig. 1). Deep-water sediments of the Gulf of Mexico are essentially biogenic with a predominance of silty clay and are impoverished in organic material (Botello et al., 2015; Kasper-Zubillaga et al., 2019).

CLIMATE AND SIMPLIFIED GEOLOGY

The Gulf of Mexico climate is considered as sub-humid to humid (Tamayo, 1991; Salas-Monreal et al., 2018). There are three well-defined climatic conditions in the Gulf of Mexico:

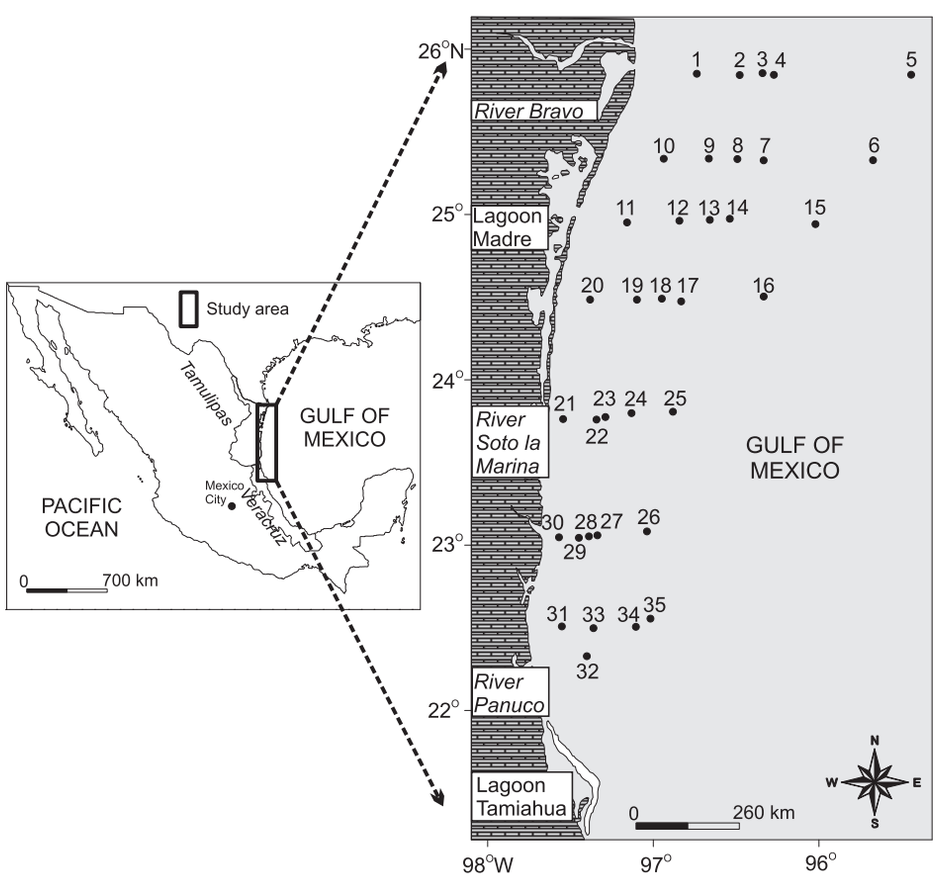

Fig. 1. Simplified map of the study area showing sample locations in the NW Gulf of Mexico (map modified after Botello et al., 2015)

– dry (February–May);
– rainy (June–November);
– windy (northern winds, 50–70 knots speed; Yañez-Arancibia and Day, 1982).

The outcrops along the Gulf of Mexico are composed of:
– Quaternary alluvium and soils;
– Cenozoic and Mesozoic clastic and calcareous sedimentary rocks;
– Cenozoic volcanic rocks of mafic and intermediate type;
– Paleozoic and Precambrian metamorphic rocks comprising schist and gneiss (Ortega-Gutierrez et al., 1995; Verma, 2015).

MATERIALS AND METHODS

Thirty-five near-surface sediment samples were collected during an oceanographic campaign conducted on board the R/V "Justo Sierra" in July 2010 along the continental shelf and upper slope regions of the NW Gulf of Mexico (Fig. 1). Sediment samples were recovered using a Reineck box-corer at water depths varying from ~48 to 2329 m and stored frozen in clean containers until analysis in the laboratory.

GRAIN SIZE ANALYSIS

Granulometric analysis of sediments was carried out by a *Beckman Coulter LS230* Laser diffraction particle size analyser adjusted with a range size of 0.04 and 2000 mm.

SEM-EDS

Mineral chemistry was measured by a *PHILLIPS XL-30* scanning electron microscope (SEM) equipped with energy dispersive spectrometer (EDS) at UNAM, Mexico.

GEOCHEMICAL ANALYSIS

A total of 35 sediment samples were analysed for major and trace element concentrations. A sequential *Siemens SRS 3000 X*-ray spectrometer, equipped with a 125 µm rhodium tube and a beryllium window, was used to measure the major (Al_2O_3, Fe_2O_3, MgO) and trace (Cu, Zn, and Pb) element concentrations. Errors estimated in the determinations are lower than 1% for major elements and lower than 4% for trace elements. In all cases, the calibration curves have been constructed according to international standards. The remaining major elements (SiO_2, TiO_2, MnO, CaO, MgO, Na_2O, and K_2O) were analysed by utilizing loss on ignition (LOI) performed on the cast sample (bead). Beads were prepared by mixing 1 g of powdered sample with 9 g of $Li_2B_4O_7$-$LiBO_2$ flux mix (50:50 wt.%). Before heating, two drops of LiBr in aqueous solution concentrated at 250 g/L were added.

Analysis of trace elements was performed using a pressed sample, which is prepared by profusely mixing 6 g of fine powder (particle size <74 microns) with 0.6 g of Hoechst wax C as a binding agent. The mix is pressed at 30 tons, and the pressure is sustained for 30 seconds. The device being used is a Graseby/Specac press, as well as a pellet casting die, measuring 4 cm in diameter. The die is equipped with a mechanism that evacuates gas, thus avoiding pellet surface irregularities. For sample series, one duplicate is prepared per 10 samples to verify repetition of preparation conditions.

RESULTS

MAJOR ELEMENT CONCENTRATIONS

The major element data are listed in Table 1. The major element concentrations were normalized with average upper continental crust values (UCC; Taylor and McLennan, 1985) and are shown in Figure 2. Relative to UCC the sediment samples are slightly enriched in TiO_2, Al_2O_3, MnO, and CaO contents. The variation in MnO content among sediment samples is significant, and is higher than in average UCC. The K_2O and Na_2O contents in sediments are slightly depleted relative to UCC.

Al_2O_3 content displayed a very uniform distribution, with slightly higher values at stations 3, 9, 12 and 17, with a range from ~16.2 to 16.9 wt.% (number of samples n = 35), at shallow depth (<500 m isobaths). Low concentrations of Al_2O_3 (the mean with one-standard-deviation value being 13.3 ±1.7) were observed in locations in front of the rivers Bravo, Soto La Marina, and Panuco (Fig. 3A). The average Al_2O_3 content in deep-sea sediments reported by Chester (2000) is 9.5 wt.%. However, sediments of this study displayed concentrations higher than this value (~9.5–16.9%; 13.3 ±1.7), which is probably due to the higher amount of terrigenous materials in the NW Gulf of Mexico. On the other hand, the behaviour of Fe_2O_3 (~3.58–5.81 wt.%; 5.16 ±0.47) is quite similar to that of Al_2O_3, which likely indicates its terrigenous origin (Fig. 3B). The high Fe_2O_3 contents (~5.50 to 5.81 wt.%) are observed at <500 m isobaths, in stations 3, 4, 7, 14, 17, 18, 19, 23, and 24. The Fe_2O_3 content decreases between 500 and 1500 m isobaths (5.02%) and at the mouth of the River Bravo (3.58 wt.%).

The MgO content varies between 1.69 and 2.83 wt.% (2.44 ±0.22, n = 35). The high MgO contents are observed in stations 7, 13 and 14, which vary between 500 and 1000 m isobaths and are low in the surrounding areas (Fig. 3C). The lowest MgO values are observed in stations 1 and 26 at ~1500 m isobaths (1.69 and 1.87 wt.%, respectively), which are located in front of the river mouth (River Bravo). Except station 1, the remaining stations exhibited values above the Mg baseline for deep water sediments proposed by Chester (2000), which is 1.8%. The high MgO contents at stations 7, 13, and 14 are probably due to the concentration of organic matter, which tends to trap certain metals to form chelates (Table 1).

The correlation between SiO_2 and Al_2O_3 is statistically not significant at 99% confidence level (r = –0.34, n = 35; critical t value for 99% confidence level is 0.418; Verma, 2005), indicating that SiO_2 content is mainly controlled by quartz (Nagarajan et al., 2015, 2017). Similarly, a statistically insignificant correlation between Al_2O_3 and TiO_2 contents (r = 0.39, n = 35) suggests that clay minerals are not the main controller of TiO_2 concentration in sediments (Zaid and Gahtani, 2015; Anaya-Gregorio et al., 2018). A significant correlation between Fe_2O_3 and TiO_2 contents (r = 0.56, n = 35) probably indicates the concentration of detrital minerals like magnetite and ilmenite

Table 1

Major element concentrations [weight %] for the surficial sediments of the NW Gulf of Mexico

Sample	SiO_2	TiO_2	Al_2O_3	$Fe_2O_3^*$	MnO	MgO	CaO	Na_2O	K_2O	P_2O_5	LOI	Total	CIA
1	69.9	0.505	9.49	3.58	0.045	1.69	2.65	2.01	2.12	0.071	7.83	99.9	75
2	53.0	0.612	15.0	5.27	0.079	2.58	3.59	3.61	2.53	0.136	13.4	99.8	80
3	50.5	0.619	16.5	5.80	0.072	2.36	4.18	3.20	2.78	0.149	13.8	100.0	81
4	50.2	0.622	15.2	5.55	0.218	2.47	4.03	4.14	2.83	0.149	14.5	99.9	76
5	40.5	0.491	11.0	4.76	0.323	2.38	13.8	3.09	2.28	0.131	21.0	99.8	43
6	41.7	0.495	10.7	4.93	0.545	2.16	12.6	3.41	2.31	0.126	21.0	99.9	43
7	49.4	0.596	13.2	5.81	0.163	2.68	5.73	4.11	2.80	0.153	15.2	99.9	65
8	48.6	0.595	14.5	5.28	0.058	2.42	7.39	3.17	2.66	0.128	15.1	99.9	66
9	52.1	0.601	16.5	5.38	0.094	2.28	3.56	3.67	2.61	0.136	12.8	99.7	83
10	56.8	0.648	13.4	5.19	0.069	2.63	3.43	3.19	2.71	0.131	11.7	99.9	77
11	56.2	0.655	13.0	5.17	0.063	2.64	3.81	3.35	2.72	0.117	12.3	100.0	73
12	51.8	0.608	16.9	5.42	0.125	2.23	3.68	3.35	2.54	0.142	13.0	99.8	84
13	48.9	0.589	12.9	5.29	0.08	2.66	7.79	3.18	2.69	0.136	15.5	99.7	60
14	49.6	0.602	13.2	5.57	0.087	2.67	6.46	3.49	2.80	0.139	14.8	99.4	64
15	42.9	0.520	11.7	4.99	0.336	2.40	12.5	2.98	2.36	0.126	19.2	100.0	47
16	41.6	0.501	13.0	4.87	0.304	2.38	12.2	3.09	2.24	0.127	19.4	99.7	51
17	47.7	0.564	16.2	5.79	0.156	2.22	5.65	3.80	2.48	0.154	15.1	99.9	74
18	50.1	0.615	12.9	5.51	0.089	2.75	6.04	3.59	2.79	0.137	15.1	99.6	64
19	52.6	0.645	13.1	5.51	0.094	2.83	4.86	3.53	2.75	0.122	14.1	100.0	69
20	54.7	0.636	13.4	5.25	0.063	2.28	4.94	2.92	2.63	0.137	13.0	99.9	72
21	55.8	0.612	11.8	4.66	0.083	2.46	5.71	3.01	2.56	0.139	13.4	100.0	64
22	52.5	0.632	12.8	5.40	0.071	2.68	5.09	3.54	2.73	0.146	14.3	99.9	67
23	50.2	0.619	13.8	5.51	0.171	2.67	5.10	3.65	2.62	0.139	15.2	99.7	70
24	49.7	0.591	14.4	5.69	0.053	2.62	5.96	3.22	2.76	0.132	14.9	100.0	69
25	45.6	0.543	12.2	5.21	0.433	2.54	10.2	3.13	2.48	0.136	17.4	99.9	53
26	44.3	0.536	12.3	5.11	0.229	2.13	9.97	3.03	2.40	0.129	20.6	100.7	54
27	53.5	0.621	13.0	5.11	0.308	2.38	6.05	2.79	2.62	0.158	13.6	100.1	67
28	50.5	0.614	14.0	5.26	0.108	2.61	5.49	3.36	2.58	0.142	15.3	100.0	70
29	53.9	0.646	12.4	4.95	0.075	2.58	5.82	2.98	2.68	0.128	13.5	99.6	65
30	46.9	0.522	11.0	4.14	0.053	2.39	12.6	2.16	2.29	0.119	17.5	99.6	46
31	55.0	0.601	11.7	4.38	0.06	2.26	6.84	2.87	2.47	0.125	13.6	99.9	61
32	53.2	0.589	12.5	4.73	0.063	2.36	7.05	2.81	2.62	0.125	13.5	99.6	62
33	51.3	0.606	13.5	5.37	0.103	2.51	6.06	3.07	2.77	0.142	14.2	99.6	67
34	48.2	0.584	15.6	5.43	0.462	2.35	6.74	3.03	2.53	0.141	15.1	100.2	71
35	45.1	0.524	12.3	4.88	0.279	2.36	10.9	2.86	2.33	0.123	18.2	99.8	52
Mean	50 ±5	0.6±0.05	13 ±1.7	5 ±0.5	0.2 ±0.1	2.4 ±0.2	7 ±3	3.2 ±0.4	2.6 ±0.2	0.13 ±0.01	15 ±3	100 ±.2	65 ±11

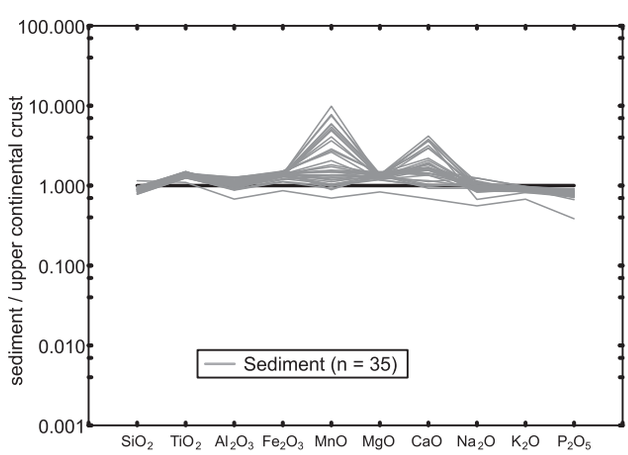

Fig. 2. Multi-element diagram of major element concentrations normalized against average upper continental crust (Taylor and McLennan, 1985)

(Armstrong-Altrin et al., 2012; Hou et al., 2017). This interpretation is further supported by the SEM-EDS analysis, in which magnetite and ilmenite are identified (Fig. 4). Based on the chemical classification diagram the sediments are classified as shale and wacke types (Fig. 5; Herron, 1988).

TRACE ELEMENT CONCENTRATIONS

The trace element concentrations are reported in Table 2 and the UCC normalized trace element patterns are shown in Figure 6. In comparison with UCC the concentrations of the surface sediment samples are generally low in Sr, Zr, Ba, Ni, and Nb. Exceptionally, sediments from a few stations are enriched in Th and Cu (Fig. 6).

The Cu content varies from 26 to 39 μgg^{-1} with a mean value of 32 ±3.9 μgg^{-1}. The highest concentrations, i.e. 46 μgg^{-1}, 39 μgg^{-1}, 38 μgg^{-1}, 36 μgg^{-1}, and 35 μgg^{-1} are recorded at stations 15, 16, 25, 26 and 35, respectively, located at >500 m isobaths (Fig. 7A). In contrast, the Cu contents are low

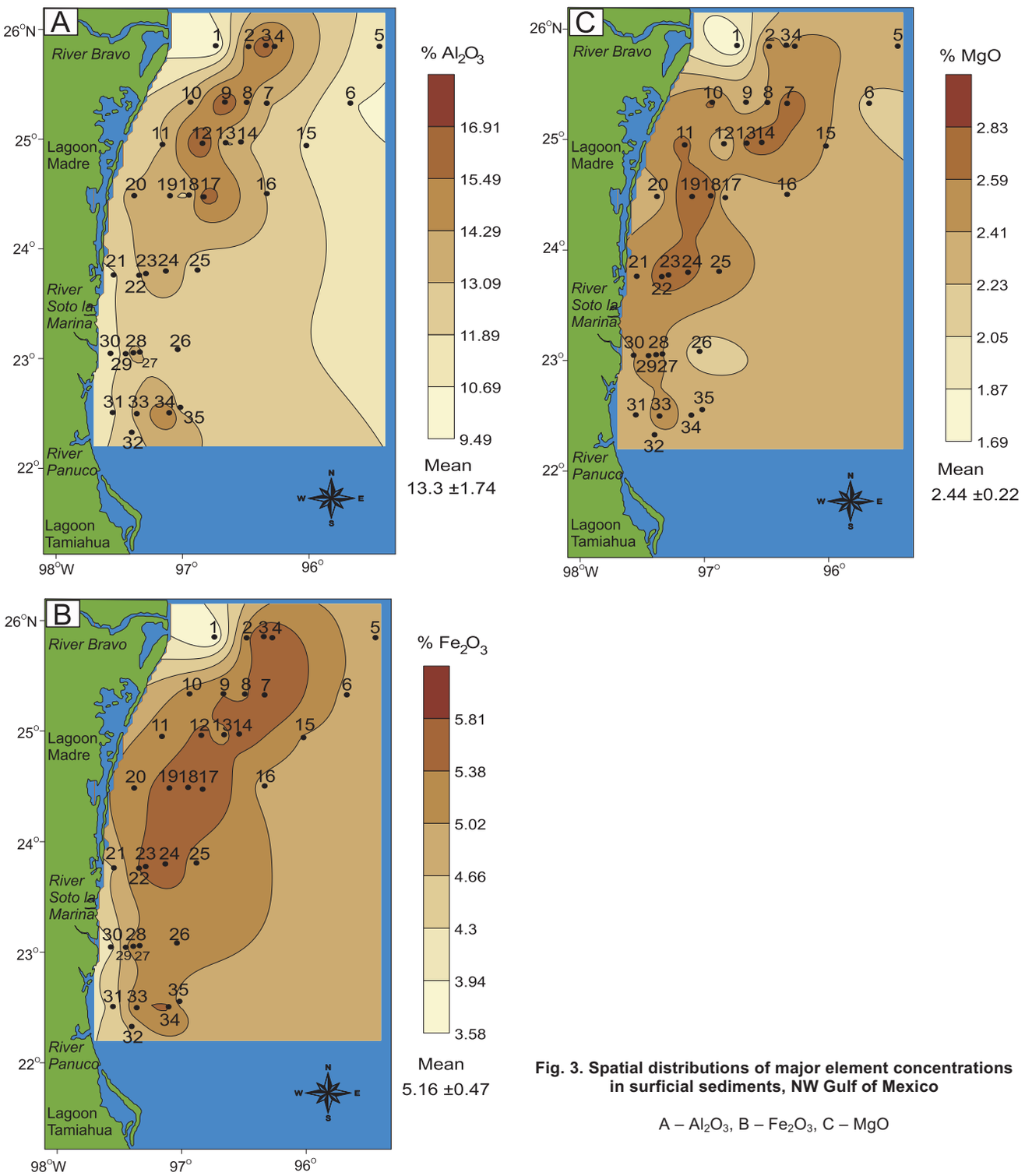

Fig. 3. Spatial distributions of major element concentrations in surficial sediments, NW Gulf of Mexico

A – Al_2O_3, B – Fe_2O_3, C – MgO

in the stations located closer to the mouth of the Rio Bravo (station 1), Madre Lagoon (station 20), and between the Soto La Marina and Panuco rivers (21, 30 and 31; Fig. 1). Similarly, the Cu content decreases as the distance from the coast increases. Cu concentrations at all stations are higher than the sediment quality guideline Effects Range Low (ERL) value for sediments reported by Long et al. (1995), which is 34 $\mu g g^{-1}$; they are, however, lower than the concentration reported by Chester (2000), which is 200 $\mu g g^{-1}$. The low Cu concentration of this study compared with the average values mentioned above indicates that the Cu is of lithogenic origin.

The Pb concentration varies from 15 to 25 $\mu g g^{-1}$, with a mean value of 20 ±3 $\mu g g^{-1}$. The Pb content is high (~23–24 $\mu g g^{-1}$), at stations 11, 19, and 23, which are located at ~ 500 m isobaths, where the sediment discharge from Madre Lagoon exerts significant detrital influence. Similarly, the Pb

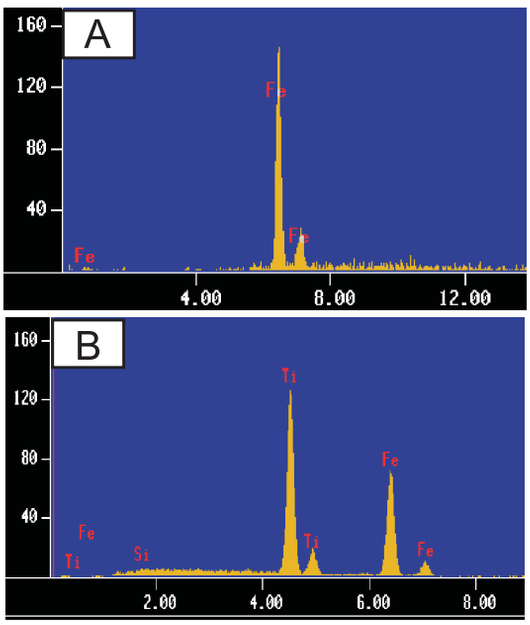

Fig. 4. SEM-EDS spectrum

A – magnetite (sample no. 1), B – ilmenite (sample no. 32)

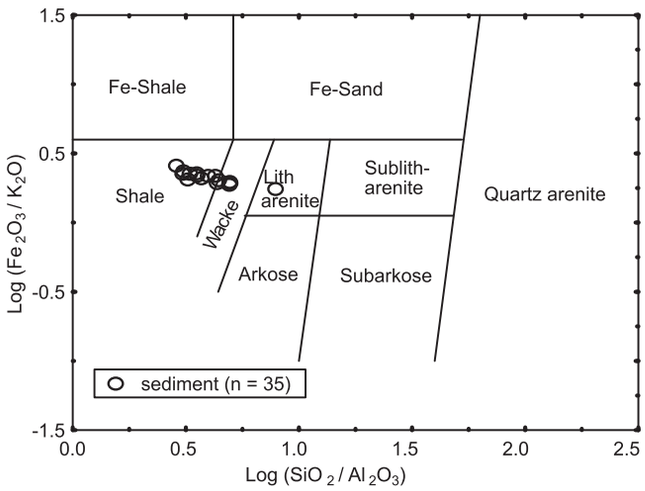

Fig. 5. Geochemical classification diagram using log (Fe_2O_3/K_2O) *versus* log (SiO_2/Al_2O_3) (Herron, 1988)

Table 2

Trace element concentrations [ppm] for the surficial sediments of the NW Gulf of Mexico

Sample	Ba	Co	Cu	Cr	Nb	Ni	Pb	Rb	Sr	Th	V	Y	Zn	Zr
1	395	13	28	116	8	22	17	95	146	10	95	25	75	211
2	403	11	31	77	12	29	23	122	178	12	135	29	107	167
3	348	10	30	87	10	30	21	119	177	10	143	27	109	142
4	357	12	33	75	10	33	24	122	181	11	139	29	114	139
5	342	15	39	54	9	39	16	95	449	8	115	24	93	127
6	360	17	46	62	9	43	15	96	427	9	127	25	98	124
7	347	13	33	71	9	35	21	118	222	10	144	27	112	127
8	326	14	30	70	11	31	21	116	280	9	134	28	107	147
9	390	11	30	100	11	29	20	116	149	10	134	28	106	148
10	464	13	31	73	12	29	22	123	148	10	129	31	109	178
11	415	11	31	89	14	29	24	121	156	10	129	31	105	180
12	372	12	31	80	8	30	23	115	133	9	133	27	109	136
13	305	11	30	94	11	31	18	112	261	9	132	26	100	142
14	350	13	32	70	11	37	17	122	251	11	145	29	112	140
15	375	16	39	56	9	41	16	100	406	9	120	26	99	129
16	334	15	38	55	9	39	15	99	405	9	114	25	97	129
17	320	13	30	78	11	32	19	113	212	10	125	27	103	134
18	305	13	31	81	6	31	19	107	146	10	123	25	106	118
19	334	11	29	69	10	30	25	119	168	10	133	28	108	144
20	404	10	29	67	12	26	22	115	157	12	129	29	101	163
21	393	12	28	61	12	25	19	109	183	12	97	29	93	191
22	356	14	29	102	10	29	23	117	147	10	115	30	106	143
23	336	13	32	66	12	31	25	121	183	12	134	30	109	143
24	331	10	32	73	12	31	19	118	210	11	127	27	106	136
25	372	13	36	81	9	36	15	104	330	9	121	25	98	128
26	366	13	36	58	10	35	15	105	338	10	113	27	98	133
27	338	12	30	72	8	28	20	105	152	10	111	27	96	168
28	357	12	30	98	9	28	21	111	145	10	110	27	101	139
29	355	11	30	117	11	28	20	111	156	11	120	29	97	162
30	296	12	26	54	9	23	16	89	492	7	95	25	81	187
31	338	12	29	60	11	26	18	104	185	10	92	28	88	189
32	308	12	30	71	11	25	22	108	198	10	102	28	96	168
33	316	13	31	69	5	28	21	100	122	8	121	24	100	117
34	330	12	32	65	10	32	23	112	217	11	120	28	106	141
35	336	13	35	59	9	34	20	99	344	7	105	24	95	131
Mean	353±36	12 ±2	31 ±3	75 ±17	10 ±2	31 ±5	20 ±3	110 ±9	230 ±103	10 ±1	121 ±14	27 ±2	101 ±8	148 ±23

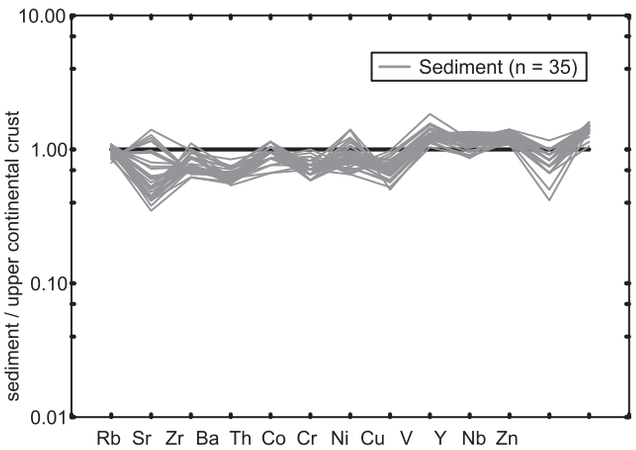

Fig. 6. Multi-element diagram of trace element concentrations normalized against average upper continental crust (Taylor and McLennan, 1985)

concentration decreases in stations farther away from the coast (Fig. 7B). The Pb concentrations at all 35 stations are below the ERL value reported for marine sediments (46.7 $\mu g g^{-1}$; Long et al., 1995), as well as the average value (200 $\mu g g^{-1}$) reported by Chester (2000). The distribution of Zn in sediments varies from 75 to 114 $\mu g g^{-1}$ with a mean value of 101 ±8 $\mu g g^{-1}$. The stations that recorded the highest Zn contents are located at ~500 m isobaths. Also, except stations 1, 30, 31 and 32, located near to the coast, other stations recorded Zn concentrations between 100 and 114 $\mu g g^{-1}$ (Fig. 7C). The Zn contents of this study are below the ERL value of marine sediments reported by Long et al. (1995) and Chester (2000), which is 150 $\mu g g^{-1}$. Hence, the low Zn content of this study may suggest that the origin of Zn is terrigenous. The average values of transition trace elements Cr (75 ±16) and Ni (31 ±5) are also near to the ERL values of marine sediments (81 and 20.9 $\mu g g^{-1}$, respectively) reported by Long et al. (1995), indicating terrigenous origin (Ramos-Vázquez et al., 2018; Taheri et al., 2018). A wide variation in Zr (~117–211 $\mu g g^{-1}$) and Sr (~122–449 $\mu g g^{-1}$) contents in sediments among stations probably indicates the fractionation of minerals during transportation and deposition (Tapia-Fernandez et al., 2017).

DISCUSSION

WEATHERING CONDITION IN THE SOURCE AREA

The degree of alteration of feldspars to clays indicates both the degree of weathering of source rocks and that of the diagenesis experienced by the sediments since deposition (Nesbitt et al., 1997; Liu et al., 2016; Yang and Du, 2017). Various weathering indices have been developed and are extensively used by researchers to identify the chemical weathering intensity of the source area (e.g., Price and Velbel, 2003; Lee, 2009; Armstrong-Altrin et al., 2014). Some examples are weathering index of Parker (WIP; Parker, 1970), chemical index of weathering (CIW; Harnois, 1988), chemical index of alteration (CIA; Nesbitt and Young 1982) and Plagioclase index of alteration (PIA; Fedo et al., 1995). Among these weathering indices, a chemical index widely used to determine the degree of source area weathering is the chemical index of alteration (CIA; Paikaray et al., 2008; Madhavaraju et al., 2016, 2017; Yang and Du, 2017; Kelepile et al., 2017; Wang et al., 2017, 2018; Armstrong-Altrin et al., 2018). This can be calculated using the formula (molecular proportions):

$$CIA = [Al_2O_3/(Al_2O_3 + CaO^* + Na_2O + K_2O)] \times 100$$

where: CaO^* is the amount of CaO incorporated in the silicate fraction of the rock.

In general, the Ca content in sediments is sourced from inorganic carbon and Na may be associated with sea-salt. The Ca content in the silicate fraction was calculated by the equation (Martinez et al., 2010):

$$Ca = CaO_t – CaO_{trg} \text{ and } CaO_{trg} = Al_2O_{3t} \times (CaO/Al_2O_3)_{UCC}$$

where: "t" = the total abundance in the sample and "trg" = terrigenous.

Similarly, excess Na (Na_{excess}) in sediments was calculated by the equation:

$$Na_{excess} = (Na_2O \times 0.7419) – (0.1 \times Al_2O_3 \times 0.5292)$$

where: Na_{excess} is the pore water salt component of Na (Murray and Leinen 1996; Armstrong-Altrin and Machain-Castillo, 2016).

According to Nesbitt and Young (1982), CIA values of unaltered plagioclase and K-feldspar are approximately equal to 50 and higher CIA values (>70) are indicative of intense chemical weathering. The CIA values for the sediment samples range from ~43 to 84, which indicate a moderate to high intensity of chemical weathering in the source area (Table 1). This result is also in agreement with the slightly elevated Rb/Sr ratios (>1) of the surface sediments (~0.84–1.13), because intensive chemical weathering may lead to increase the Rb/Sr ratio, and high ratios (>1) are indicators of intense weathering (McLennan et al., 1993).

SEDIMENT PROVENANCE

The discriminant function diagram proposed by Roser and Korsch (1988) is frequently used by many researchers to infer sediment provenance (Tawfik et al., 2017, 2018). This diagram helps to discriminate four provenance categories, i.e., mafic (P1), intermediate (P2), felsic (P3) and quartzose recycled (P4). On this diagram, sediment samples plot in the intermediate igneous provenance field (Fig. 8). It seems that the surface sediments of the NW Gulf of Mexico were derived mostly from the contribution of intermediate igneous rocks (e.g., andesite). Similarly, based on the $(SiO_2)_{adj}$ content the sediments are classified mainly as of intermediate type (Fig. 9; Le Bas et al., 1986; Armstrong-Altrin, 2009), which is consistent with our interpretation based on the Roser and Korsch (1988) provenance classification.

High concentrations of Cr (>150 ppm) and Ni (>100 ppm) in sediments are suggestive of ultramafic rocks in the source area (Garver et al., 1996; Armstrong-Altrin et al., 2004). The Cr and Ni contents in the sediments vary between ~54–117 ppm and ~22–43 ppm, respectively, indicating that the sediments were likely derived from intermediate rocks (Table 2). In addition, in the ternary diagram of Ni-Th*10-V the sediments plot near to the average composition of andesite, which also suggests that the sediments were derived by the weathering of intermediate

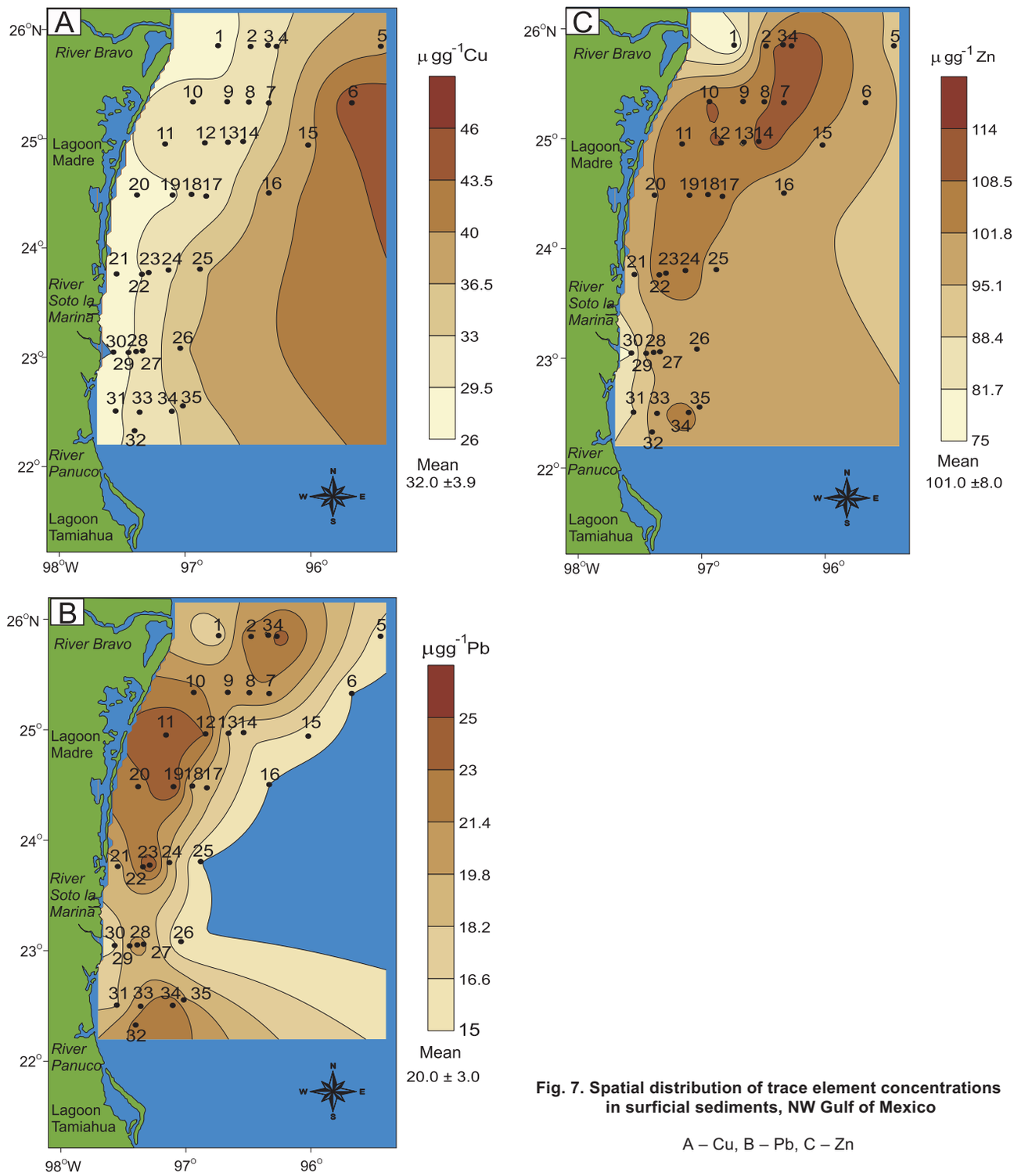

Fig. 7. Spatial distribution of trace element concentrations in surficial sediments, NW Gulf of Mexico

A – Cu, B – Pb, C – Zn

rocks (Bracciali et al., 2007; Fig. 10). Average geochemistry data of the probable source rocks plotted in Figure 10 are compiled from Verma (1999, 2000, 2001a, b), Carrasco-Núñez et al. (2005), and Schaaf et al. (2005), which are located along the coastal areas of the Gulf of Mexico.

PALAEO-OXYGENATION CONDITION

In many studies, the V/Cr ratio has been used as an index to identify the paleo-oxygenation condition (Dill et al., 1988; Jones and Manning, 1994; Morford and Emerson, 1999; Hu et al., 2017; Bansal et al., 2018). Cr is mainly incorporated in the detrital fraction of sediments, and it may substitute for Al in the clay structure (Riquier et al., 2006). Vanadium may be bound to organic matter by the incorporation of V^{4+} into porphyrins, and is found in sediments deposited under reducing environments (Shaw et al., 1990). If the values are >2, it indicates anoxic conditions, whereas values <2 suggest more oxidizing conditions (Jones and Manning, 1994). In the present study, the average V/Cr ratio in the sediments (~0.82–2.14; 1.68 ±0.33) is generally <2, which indicates that these sediments were deposited

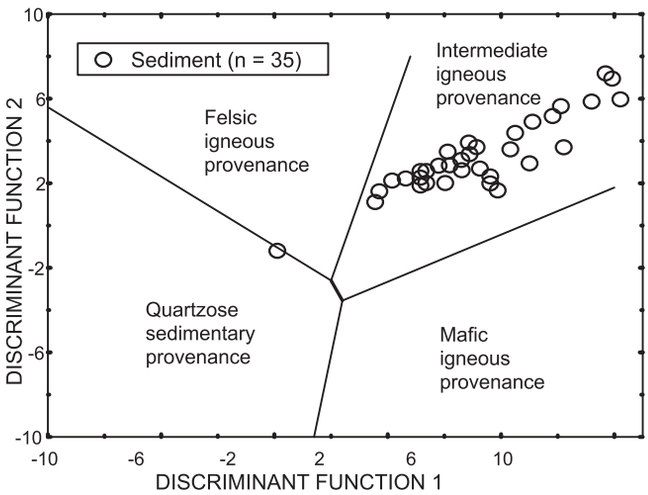

Fig. 8. Major element provenance discriminant function diagram for the sediments (Roser and Korsch, 1988)

The discriminant functions are: discriminant function 1 = (–1.773 · TiO_2) + (0.607 · Al_2O_3) + (0.760 · Fe_2O_3) + (–1.500 · MgO) + (0.616 · CaO) + (0.509 · Na_2O) + (–1.224 · K_2O) + (–9.090); discriminant function 2 = (0.445 · TiO_2) + (0.070 · Al_2O_3) + (–0.250 · Fe_2O_3) + (–1.142 · MgO) + (0.438 · CaO) + (1.475 · Na_2O) + (1.426 · K_2O) + (–6.861)

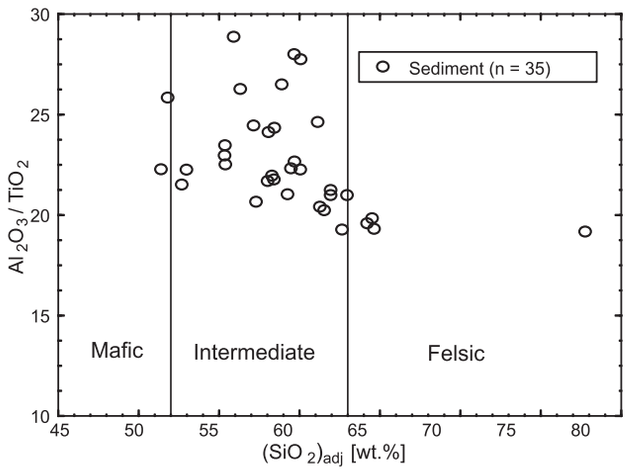

Fig. 9. The Al_2O_3/TiO_2 *versus* $(SiO_2)_{adj}$ plot of the surficial sediments, modified after Armstrong-Altrin (2009)

n = number of samples

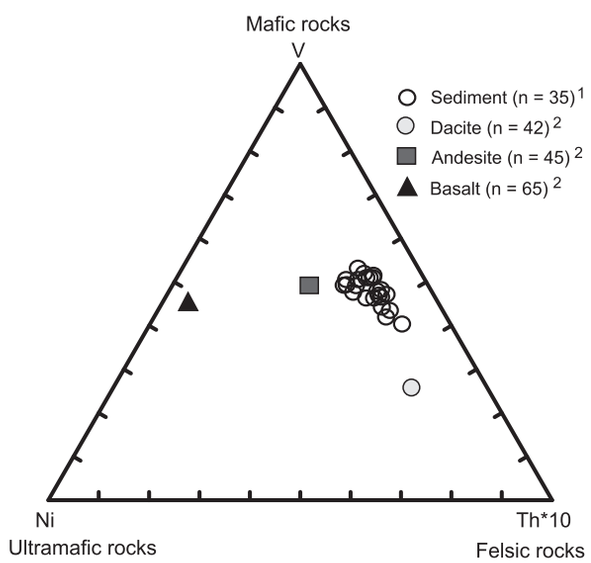

Fig. 10. Ni-Th*10-V ternary diagram of the surficial sediments from the NW Gulf of Mexico (after Bracciali et al., 2007)

1 – this study, 2 – average data for comparison are from Verma (2001a, b), Verma (2015) and Ortega-Gutierrez et al. (1995)

mostly in an oxic environment. However, slight differences in the V/Cr ratio among various stations may suggest a change in the depositional conditions or possibly variations in the oxygen level of the depositional environment.

Numerous studies have applied Ni/Co ratio as a redox indicator (Dypvik, 1984; Dill, 1986; Hua et al., 2013; Arora et al., 2015; Armstrong-Altrin and Machain-Castillo, 2016). Jones and Manning (1994) suggested that a Ni/Co ratio <5 indicates an oxic environment, whereas >5 suggests sub-oxic and anoxic environments. The Ni/Co ratios in these sediments are very low (~1.69–3.10; 2.50 ±0.30), which suggest that they were deposited in an oxygenated environment. According to Hallberg (1976), the high Cu/Zn ratio (>1) indicates a redox depositional condition, while low Cu/Zn ratio (<1) suggests an oxic condition. The low Cu/Zn ratios (~0.26–0.46; 0.32 ±0.05) in the sediment samples indicate that the sediments were deposited in a well-oxidized condition.

STATISTICAL ANALYSIS

PEARSON CORRELATION

To evaluate the association among various elements in the surficial sediments, a Pearson correlation analysis was performed. A statistically significant correlation of Al_2O_3, Fe_2O_3 and MgO was observed with Pb, Zn and OM concentrations (r = 0.54, 0.72, and 0.43, r = 0.44, 0.92, and 0.39, and r = 0.40, 0.57 and 0.51, respectively, n = 35); this implies continental derivation of trace elements combined with terrigenous materials. A significant correlation obtained between MnO and CaO (r = 0.61) indicates its derivation from a similar source, most probably biogenic. On the other hand, Fe_2O_3 and Zn showed an insignificant correlation with sand percentage (r = –0.51 and –0.36, respectively; n = 35), which indicates that these elements have no affinity with coarse-grained materials. OM did not show significant correlation with sand, silt, and clay (r = –0.14, 0.15, and –0.13, respectively), whereas it is significant against Al_2O_3 (r = 0.43, n = 35), Fe_2O_3 (r = 0.39), MgO (r = 0.41), Pb (r = 0.51), and Zn (r = 0.37, n = 35), which suggests that in some cases it may form chelates. A statistically insignificant correlation between sand and clay (r = –0.72, n = 35) may correspond to grain size variations (Table 3).

CLUSTER ANALYSIS

Cluster analysis is an exploratory data technique employed to classify groups and subgroups based on the similarities and dissimilarities among variables (Hair et al., 2001; Verma, 2005).

Displayed groups are set by variables (Fig. 11). Practically, one single group is observed in which a greater similarity among concentrations of Al_2O_3, Pb, CaO, Fe_2O_3, MgO, OM, MnO, and sand is identified, due to their terrigenous origin and to the high affinity of these elements with OM particles to form chelates. These variables exhibited very similar spatial distribution, with accumulation towards shallow waters (Figs. 3A–C and 7A–C). The subgroup of silt and Zn was amalgamated to this group, suggesting that some of the elements mentioned are transported in fine-grained (silt) particles present in the sediments. Another subgroup was amalgamated to the one mentioned previously, in which concentrations of Cu are linked to percentages of clay; this group was dominated by fine particles, to which Cu showed a high affinity. As a result, it was highly dissimilar to the main group of terrigenous materials (Fig. 11).

Table 3

Pearson correlation matrix for major elements, trace metals, organic matter (OM in %), and textural parameters (sand, silt, and clay in %) in the surficial sediments, NW Gulf of Mexico (n = 35; p ≤0.050)

	Al_2O_3	CaO	Fe_2O_3	MgO	MnO	Pb	Cu	Zn	Sand	Silt	Clay	OM
Al_2O_3	1.00											
CaO	0.51	1.00										
Fe_2O_3	0.74	–0.32	1.00									
MgO	0.17	–0.13	0.57	1.00								
MnO	–0.15	0.61	0.01	–0.20	1.00							
Pb	0.54	–0.72	0.44	0.40	–0.37	1.00						
Cu	–0.24	0.66	0.04	–0.13	0.80	–0.48	1.00					
Zn	0.72	–0.40	0.92	0.60	–0.04	0.57	0.06	1.00				
Sand	–0.27	–0.05	–0.51	–0.32	–0.09	–0.04	–0.09	–0.36	1.00			
Silt	0.17	–0.43	–0.10	–0.16	–0.18	0.37	–0.26	0.09	0.66	1.00		
Clay	–0.13	0.40	0.14	0.18	0.18	–0.34	0.25	–0.04	–0.72	–1.00	1.00	
% OM	0.43	–0.52	0.39	0.41	–0.54	0.51	–0.63	0.37	–0.14	0.15	–0.13	1.00

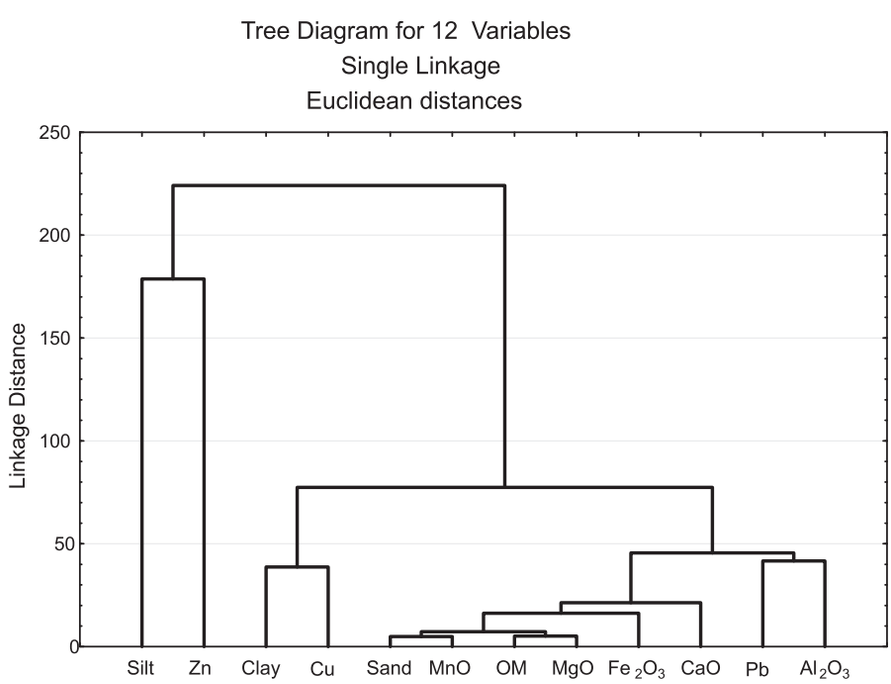

Fig. 11. Dendrogram for the variables measured in the sediments

Metrics used: pearson correlation; type of amalgamation: distant neighbours

PRINCIPAL COMPONENT ANALYSIS

PCA is a statistical technique used to identify important factors that explain the variance of a system (Ouyang, 2005). This analysis was performed to evaluate the possible provenance of trace metals, for which three factors explain 82% of system characteristics (Table 4). Upon application of the varimax rotation function for each factor, interpretation can be given, and statistical loads were determined.

The first factor showed three significant variables that explain 39% of the variance. The Al_2O_3 and Fe_2O_3 contents in the sediments are primarily of terrigenous origin, derived by the weathering of rocks mainly composed of aluminosilicates (Ramos-Vázquez et al., 2017). This first factor was accordingly designated as "terrigenous input" and was supported both by the Pearson correlation analyses and the association of the main group in cluster analysis. The loading of Zn with Al_2O_3 and Fe_2O_3 contents in factor 1 also indicates the association of Zn with aluminosilicates.

The second factor also provided three significant variables, explaining 30% of sediment characteristics such as the quantity of sand, silt, and clay. Texturally, the sediments are classified as clayey silt, which was homogeneous, and did not show a significant difference between the continental shelf and slope areas or with respect to water depth (Fig. 12).

In the third factor, two significant observable variables explain 13% of the characteristics of the system, i.e., the percentage of OM and Cu concentrations. Cu is of lithogenic origin rather than being associated with another source, which may be the reason that factor 3, did not explain the significance of these variables (Table 4). However, through the correlation matrix, it can be inferred that the significant loads of these variables in both statistical methods are a result of the absence of affinity between Cu and OM. Thus, OM did not capture this metal or form chelates with it.

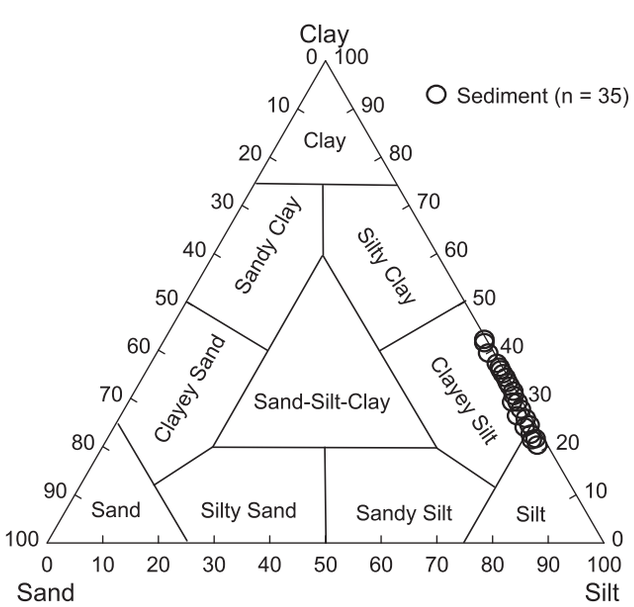

Fig. 12. Sand–silt–clay ternary diagram for the surficial sediments, NW Gulf of Mexico (modified after Shepard, 1954)

Table 4

Factor analysis through main components, varimax rotation; significant loads >0.70

Variables	Factor 1	Factor 2	Factor 3
Al_2O_3	0.790514	0.132282	0.210483
CaO	0.403417	0.336511	–0.2111251
Fe_2O_3	0.950813	–0.181918	0.050831
MgO	0.555961	–0.287189	0.323296
MnO	–0.008650	0.020346	0.189308
Pb	0.571065	0.305382	0.541147
Cu	0.087294	–0.162583	–0.927810
Zn	0.977789	0.011312	–0.035203
Sand	–0.402557	0.790460	–0.046612
Silt	0.075502	0.965295	0.128449
Clay	–0.027445	–0.978439	–0.114173
% OM	0.343190	0.007837	0.819451
Variance	3.413190	2.766915	2.009526
% factor	39.09824	29.54873	13.24934
% accumulated	39.09824	68.64698	81.89631

HEAVY METAL CONTAMINATION

ENRICHMENT FACTOR

A number of researchers have proposed the use of Enrichment factors (EF) to quantify the degree of anthropogenic influence in sediments (Selvaraj et al., 2004; Acevedo et al., 2006; Armstrong-Altrin et al., 2015a; Khan et al., 2017; Anaya-Gregorio et al., 2018), which can be calculated according to the formulae:

$$EF = (M/Al)_{sample}/(M/Al)_{crust},$$

where: M is the value of analysed metal concentration (Wedepohl, 1995).

Among other major elements, we preferred Al_2O_3 content as a reference for normalization, because Al_2O_3 is considered as an immobile element, which represents the clay fraction in sediment (Prabakaran et al., 2019). If an enrichment factor is equal to one, the metals are considered as a natural source, if it is >2 it suggests an anthropogenic input. EF values are calculated based on average UCC concentrations (Taylor and McLennan, 1985) for the elements Ba, Co, Cu, Cr, Ni, Pb, Sr, V, and Zn. The EF values are lower than 2, which indicate that there is no significant anthropogenic input (Table 5). This corroborates with our interpretations based on statistical methods; neither enriched nor moderately enriched, and metal concentration was equal to the values expected under natural circumstances.

Table 5

Enrichment Factor (EF; Wedepohl, 1995) values for the surficial sediments, NW Gulf of Mexico, calculated based on average UCC values (Taylor and McLennan, 1985)

Sample	Ba	Co	Cu	Cr	Ni	Pb	Sr	V	Zn
1	1.15	1.22	1.79	2.24	0.80	1.60	0.67	1.42	1.69
2	0.74	0.66	1.26	0.94	0.67	1.37	0.52	1.28	1.53
3	0.58	0.54	1.10	0.97	0.63	1.14	0.47	1.23	1.41
4	0.65	0.71	1.32	0.90	0.75	1.41	0.52	1.30	1.60
5	0.86	1.22	2.15	0.90	1.22	1.30	1.77	1.48	1.81
6	0.93	1.42	2.61	1.06	1.39	1.25	1.73	1.69	1.96
7	0.73	0.88	1.52	0.98	0.92	1.42	0.73	1.55	1.82
8	0.62	0.86	1.26	0.88	0.74	1.29	0.84	1.31	1.58
9	0.65	0.60	1.10	1.11	0.61	1.08	0.39	1.15	1.37
10	0.96	0.87	1.41	1.00	0.75	1.47	0.48	1.37	1.74
11	0.88	0.76	1.45	1.25	0.77	1.65	0.52	1.41	1.73
12	0.61	0.63	1.11	0.87	0.61	1.22	0.34	1.12	1.38
13	0.65	0.76	1.41	1.33	0.83	1.25	0.88	1.45	1.66
14	0.73	0.88	1.47	0.97	0.97	1.15	0.83	1.56	1.82
15	0.89	1.22	2.03	0.88	1.21	1.22	1.51	1.46	1.81
16	0.71	1.03	1.78	0.77	1.04	1.03	1.35	1.25	1.60
17	0.55	0.72	1.13	0.88	0.68	1.05	0.57	1.10	1.36
18	0.65	0.90	1.46	1.15	0.83	1.32	0.49	1.35	1.76
19	0.70	0.75	1.35	0.96	0.79	1.71	0.56	1.44	1.76
20	0.83	0.67	1.32	0.92	0.67	1.47	0.51	1.37	1.61
21	0.92	0.91	1.44	0.95	0.73	1.44	0.67	1.17	1.69
22	0.77	0.98	1.38	1.46	0.78	1.61	0.50	1.28	1.77
23	0.67	0.84	1.41	0.88	0.78	1.62	0.58	1.38	1.69
24	0.63	0.62	1.35	0.93	0.74	1.18	0.63	1.25	1.57
25	0.84	0.95	1.79	1.22	1.02	1.10	1.17	1.41	1.72
26	0.82	0.94	1.78	0.86	0.98	1.09	1.19	1.30	1.70
27	0.72	0.82	1.40	1.01	0.74	1.37	0.51	1.21	1.58
28	0.70	0.77	1.30	1.28	0.69	1.34	0.45	1.12	1.54
29	0.79	0.79	1.47	1.73	0.78	1.44	0.55	1.37	1.67
30	0.74	0.97	1.44	0.90	0.72	1.30	1.94	1.23	1.58
31	0.80	0.92	1.51	0.94	0.77	1.37	0.69	1.12	1.61
32	0.68	0.86	1.46	1.04	0.69	1.57	0.69	1.16	1.64
33	0.65	0.86	1.40	0.94	0.72	1.39	0.39	1.27	1.58
34	0.58	0.69	1.25	0.76	0.71	1.32	0.60	1.09	1.45
35	0.75	0.94	1.73	0.88	0.95	1.45	1.21	1.21	1.65
Mean	0.75 ±0.1	0.86 ±0.2	1.5 ±0.3	1.1 ±0.3	0.8 ±0.2	1.3 ±0.2	0.8 ±0.4	1.3 ±0.1	1.6 ±0.1

GEO-ACCUMULATION INDEX

Geo-accumulation index (I_{geo}) can be calculated by an equation, $\log_2 (C_n/1.5 \times B_n)$ (Müller, 1969, 1979), where C_n is the measured concentration of the metal "n" in the sediment sample, B_n is the geochemical background concentration of metal "n". The I_{geo} value of 1.5 is a factor that considers possible variability generated by lithological variations. The I_{geo} consists of seven grades, i.e. Class 0 (I_{geo} = <0, practically uncontaminated), Class 1 (I_{geo} = <1, uncontaminated to moderately contaminated), Class 2 (I_{geo} = between 1 and 2; moderately contaminated), Class 3 (I_{geo} = 2–3, moderately to highly contaminated), Class 4 (I_{geo} = 3–4, highly contaminated), Class 5 (I_{geo} = 4–5, highly to extremely contami-

Table 6

Geo-accumulation Index (I_{geo}; Müller, 1979) values for the surficial sediments, NW Gulf of Mexico, calculated based on average UCC values (Taylor and McLennan, 1985)

Sample	Ba	Co	Cu	Cr	Ni	Pb	Sr	V	Zn
1	–1.06	–0.97	–0.42	–0.10	–1.58	–0.58	–1.85	–0.76	–0.51
2	–1.03	–1.21	–0.27	–0.69	–1.19	–0.15	–1.56	–0.25	0.01
3	–1.25	–1.35	–0.32	–0.52	–1.14	–0.28	–1.57	–0.17	0.03
4	–1.21	–1.09	–0.18	–0.73	–1.00	–0.09	–1.54	–0.21	0.10
5	–1.27	–0.77	0.06	–1.21	–0.76	–0.67	–0.23	–0.48	–0.20
6	–1.20	–0.58	0.29	–1.01	–0.62	–0.77	–0.30	–0.34	–0.12
7	–1.25	–0.97	–0.18	–0.81	–0.92	–0.28	–1.24	–0.16	0.07
8	–1.34	–0.87	–0.32	–0.83	–1.09	–0.28	–0.91	–0.26	0.01
9	–1.08	–1.21	–0.32	–0.32	–1.19	–0.35	–1.82	–0.26	–0.01
10	–0.83	–0.97	–0.27	–0.77	–1.19	–0.21	–1.83	–0.32	0.03
11	–0.99	–1.21	–0.27	–0.48	–1.19	–0.09	–1.75	–0.32	–0.02
12	–1.15	–1.09	–0.27	–0.64	–1.14	–0.15	–1.98	–0.27	0.03
13	–1.44	–1.21	–0.32	–0.41	–1.09	–0.50	–1.01	–0.28	–0.09
14	–1.24	–0.97	–0.23	–0.83	–0.83	–0.58	–1.06	–0.15	0.07
15	–1.14	–0.67	0.06	–1.15	–0.69	–0.67	–0.37	–0.42	–0.11
16	–1.30	–0.77	0.02	–1.18	–0.76	–0.77	–0.37	–0.49	–0.13
17	–1.37	–0.97	–0.32	–0.67	–1.04	–0.42	–1.31	–0.36	–0.05
18	–1.44	–0.97	–0.27	–0.62	–1.09	–0.42	–1.85	–0.38	–0.01
19	–1.30	–1.21	–0.37	–0.85	–1.14	–0.03	–1.64	–0.27	0.02
20	–1.03	–1.35	–0.37	–0.89	–1.34	–0.21	–1.74	–0.32	–0.08
21	–1.07	–1.09	–0.42	–1.03	–1.40	–0.42	–1.52	–0.73	–0.20
22	–1.21	–0.87	–0.37	–0.29	–1.19	–0.15	–1.84	–0.48	–0.01
23	–1.30	–0.97	–0.23	–0.92	–1.09	–0.03	–1.52	–0.26	0.03
24	–1.32	–1.35	–0.23	–0.77	–1.09	–0.42	–1.32	–0.34	–0.01
25	–1.15	–0.97	–0.06	–0.62	–0.87	–0.77	–0.67	–0.41	–0.12
26	–1.17	–0.97	–0.06	–1.10	–0.92	–0.77	–0.64	–0.51	–0.12
27	–1.29	–1.09	–0.32	–0.79	–1.24	–0.35	–1.79	–0.53	–0.15
28	–1.21	–1.09	–0.32	–0.35	–1.24	–0.28	–1.86	–0.55	–0.08
29	–1.22	–1.21	–0.32	–0.09	–1.24	–0.35	–1.75	–0.42	–0.13
30	–1.48	–1.09	–0.53	–1.21	–1.52	–0.67	–0.09	–0.76	–0.39
31	–1.29	–1.09	–0.37	–1.05	–1.34	–0.50	–1.50	–0.80	–0.28
32	–1.42	–1.09	–0.32	–0.81	–1.40	–0.21	–1.41	–0.65	–0.15
33	–1.38	–0.97	–0.27	–0.85	–1.24	–0.28	–2.11	–0.41	–0.09
34	–1.32	–1.09	–0.23	–0.94	–1.04	–0.15	–1.27	–0.42	–0.01
35	–1.30	–0.97	–0.10	–1.08	–0.96	–0.35	–0.61	–0.61	–0.16
Mean	–1.2 ±0.1	–1 ±0.2	–0.2 ±0.2	–0.8 ±0.3	–1.1 ±0.2	–0.4 ±0.2	–1.3 ±0.6	–0.4 ±0.2	–0.1 ±0.1

nated). The I_{geo} values calculated for the surficial sediments are <0 and within Class 0 (practically uncontaminated; Table 6). This interpretation is consistent with EF values, which indicates that the concentration of heavy metals in sediments is not due to an anthropogenic source.

CONCLUSIONS

1. The major element concentrations indicated that the sediments were derived from an intermediate rock composition, probably andesite located along the coastal areas of the NW Gulf of Mexico.

2. The weathering indices demonstrated that the sediments were derived from moderately to highly weathered source area.

3. Major and trace element concentrations in the surface sediments are statistically shown to be of lithogenic origin, chiefly brought into the marine depositional environment by rivers. The Rio Bravo and Soto La Marina rivers played an important role in delivering sediments to the study area.

4. The Cr, Cu, and V contents also reveal that the sediments received a major contribution from intermediate source rocks. The V/Cr, Ni/Co, and Cu/Zn ratios in sediments from the NW Gulf of Mexico are <2, <5, and <1, respectively, which support that these sediments were deposited in well-oxygenated conditions.

5. The EF for Ba, Co, Cu, Cr, Ni, Pb, Sr, V, and Zn are <2. This indicates a low probability of anthropogenic input, because they are neither enriched nor moderately enriched, and are similar to the values expected under natural circumstances. The statistical parameters also indicate the association of these elements with detrital constituents.

Acknowledgements. Financial support for this study was provided by the Instituto Nacional de Ecología y Cambio Climatico (INECC) as part of a long-term project "Marco ambiental de las condiciones oceanograficas en el sector NW de la ZEE de Mexico en el Golfo de Mexico (MARZEE)". JSA is grateful to the CONACyT Ciencia Básica (A1-S-21287) and Programa de Apoyo a Proyectos de Investigación e Innovación Tecnológica (IN106117) projects. The authors express their gratitude to the crew members of the "R/V Justo Sierra" and the scientific party that participated in this project. We are thankful to M.A. Ramos-Vázquez, Posgrado en Ciencias del Mar y Limnología for the help in statistical analysis and in calculating the Enrichment Factor and Geo-accumulation index. Thanks are also extended to C. E. García-Ruelas for providing invaluable technical support and field assistance during the course of this study. We are also grateful to C. Linares-López, T. Hernández Trevioñ, and L.E. Gómez Lizárraga for mineral identification through SEM and SEM-EDS. We extend our sincere thanks to the Journal Reviewers N. Ramasamy and M. Jayagopal for their extensive comments, which improved our presentation significantly. Technical Editing by E. Dąbrowska-Jędrusik is highly appreciated.

REFERENCES

Acevedo, D., Jiménez, B., Rodríguez, C., 2006. Trace metals in sediments of two estuarine lagoons from Puerto Rico. Environmental Pollution, **141:** 336–342.

Anaya-Gregorio, A., Armstrong-Altrin, J.S., Machain-Castillo, M.L., Montiel-García, P.C., Ramos-Vázquez, M.A., 2018. Textural and geochemical characteristics of late Pleistocene to Holocene fine-grained deep-sea sediment cores (GM6 and GM7), recovered from southwestern Gulf of Mexico. Journal of Palaeogeography, **7**: 253–271.

Armstrong-Altrin, J.S., 2009. Provenance of sands from Cazones, Acapulco, and Bahía Kino beaches, Mexico. Revista Mexicana de Ciencias Geologicas, **26:** 764–782.

Armstrong-Altrin, J.S., 2015. Evaluation of two multi-dimensional discrimination diagrams from beach and deep sea sediments from the Gulf of Mexico and their application to Precambrian clastic sedimentary rocks. International Geology Review, **57:** 1446–1461.

Armstrong-Altrin, J.S., Machain-Castillo, M.L., 2016. Mineralogy, geochemistry, and radiocarbon ages of deep sea sediments from the Gulf of Mexico, Mexico. Journal of South American Earth Sciences, **71:** 182–200.

Armstrong-Altrin, J.S., Natalhy-Pineda, O., 2014. Microtextures of detrital sand grains from the Tecolutla, Nautla, and Veracruz beaches, western Gulf of Mexico, Mexico: implications for depositional environment and palaeoclimate. Arabian Journal of Geosciences, **7:** 4321–4333.

Armstrong-Altrin, J.S, Lee, Y.I., Verma, S.P., Ramasamy, S., 2004. Geochemistry of sandstones from the upper Miocene Kudankulam Formation, southern India: implications for provenance, weathering, and tectonic setting. Journal of Sedimentary Research, **74:** 285–297.

Armstrong-Altrin, J.S., Lee, Y.I., Kasper-Zubillaga, J.J., Carranza-Edwards, A., Garcia, D., Eby, N., Balaram, V., Cruz-Ortiz, N., 2012. Geochemistry of beach sands along the Western Gulf of Mexico, Mexico: implication for provenance. Chemie der Erde Geochemistry, **72:** 345–362.

Armstrong-Altrin, J.S., Nagarajan, R., Madhavaraju, J., Rosalez-Hoz, L., Lee, Y.I., Balaram, V., Cruz-Martinez, A., Avila-Ramirez, G., 2013. Geochemistry of the Jurassic and upper Cretaceous shales from the Molango Region, Hidalgo, Eastern Mexico: implications of source-area weathering, provenance, and tectonic setting. Comptes Rendus Geoscience, **345:** 185–202.

Armstrong-Altrin, J.S., Nagarajan, R., Lee, Y.I., Kasper-Zubillaga, J.J., Córdoba-Saldaña, L.P., 2014. Geochemistry of sands along the San Nicolás and San Carlos beaches, Gulf of California, Mexico: implication for provenance. Turkish Journal of Earth Sciences, **23:** 533–558.

Armstrong-Altrin, J.S., Machain-Castillo, M.L., Rosales-Hoz, L., Carranza-Edwards, A., Sanchez-Cabeza, J.A., Ruíz-Fernández, A.C., 2015a. Provenance and depositional history of continental slope sediments in the Southwestern Gulf of Mexico unraveled by geochemical analysis. Continental Shelf Research, **95:** 15–26.

Armstrong-Altrin, J.S., Nagarajan, R., Balaram, V., Natalhy-Pineda, O., 2015b. Petrography and geochemistry of sands from the Chachalacas and Veracruz beach areas, western Gulf of Mexico, Mexico: constraints on provenance and tectonic setting. Journal of South American Earth Sciences, **64:** 199–216.

Armstrong-Altrin, J.S., Lee, Y.I., Kasper-Zubillaga, J.J., Trejo-Ramírez, E., 2017. Mineralogy and geochemistry of sands along the Manzanillo and El Carrizal beach areas, southern Mexico: implications for palaeoweathering, provenance, and tectonic setting. Geological Journal, **52**: 559–582.

Armstrong-Altrin, J.S., Ramos-Vázquez, M.A., Zavala-León, A.C., Montiel-García, P.C., 2018. Provenance discrimination between Atasta and Alvarado beach sands, western Gulf of Mexico, Mexico: constraints from detrital zircon chemistry and U-Pb geochronology. Geological Journal, **53:** 2824–2848.

Arora, A., Banerjee, S., Dutta, S., 2015. Black shale in late Jurassic Jhuran Formation of Kutch. Journal of the Geological Society of India, **85:** 265–278.

Bansal, U., Banerjee, S., Ruidas, D.K., Pande, K., 2018. Origin and geochemical characterization of the glauconites in the upper Cretaceous Lameta Formation, Narmada Basin, central India. Journal of Palaeogeography, **7:** 99–116.

Basu, A., 2017. Evolution of siliciclastic provenance inquiries: a critical appraisal. In: Sediment Provenance (ed. Rajat Mazumder): 5–23. Elsevier Amsterdam, Netherlands. Chapter 2. doi:10.1016/B978-0-12-803386-9.00002-2

Botello, A.V., Soto, L.A., Ponce-Veléz, G., Villanueva, F.S., 2015. Baseline for PAHs and metals in NW Gulf of Mexico related to the Deepwater Horizon oil spill. Estuarine, Coastal and Shelf Science, **156:** 124–133.

Bracciali, L., Marroni, M., Pandolfi, L., Rocchi, S., 2007. Geochemistry and petrography of western Tethys Cretaceous sedimentary covers (Corsica and Northern Apennines): from source areas to configuration of margins. In: Sedimentary provenance and petrogenesis: Perspectives from petrography and geochemistry, vol. 420 (eds. J. Arribas, S. Critelli, M.J. Johnsson): 73–93. Geological Society of America Special Paper.

Carrasco-Núñez, G., Righter, K., Chesley, J., Siebert, L., Aranda-Gómez, J.J., 2005. Contemporaneous eruption of calc-alkaline and alkaline lavas in a continental arc (Eastern Mexican Volcanic Belt): chemically heterogeneous but isotopically homogeneous source. Contributions to Mineralogy and Petrology, **150:** 423–440.

Chaudhuri, A., Banerjee, S., Le Pera, E., 2018. Petrography of Middle Jurassic to early Cretaceous sandstones in the Kutch Basin, western India: implications on provenance and basin evolution. Journal of Palaeogeography, **7:** 2.

Chester, R., 2000. Marine Biogeochemistry. Blackwell Science Great Britain.

Cullers, R.L., 2000. The geochemistry of shales, siltstones and sandstones of Pennsylvanian-Permian age, Colorado, USA: implications for provenance and metamorphic studies. Lithos, **51:** 181–203.

Cullers. R.L., Basu, A., Suttner, L.J., 1988. Geochemical signature of provenance in sand-size material in soils and stream sediments near the Tobacco Root batholith, Montana, USA. Chemical Geology, **70:** 335–348.

Dill, H., 1986. Metallogenesis of early Paleozoic graptolite shales from the Graefenthal Horst (northern Bavaria-Federal Republic of Germany). Economic Geology, **81:** 889–903.

Dill, H., Teshner, M., Wehner, H., 1988. Petrography, inorganic and organic geochemistry of Lower Permian Carboniferous fan sequences ("Brandschiefer Series") FRG: constraints to their paleogeography and assessment of their source rock potential. Chemical Geology, **67:** 307–325.

Dypvik, H., 1984. Geochemical compositions and depositional conditions of Upper Jurassic and Lower Cretaceous Yorkshire clays, England. Geological Magazine, **121:** 489–504.

Etemad-Saeed, N., Hosseini-Barzi, M., Adabi, M.H, Sadeghi, A., Houshmandzadeh, A., 2015. Provenance of Neoproterozoic sedimentary basement of northern Iran, Kahar Formation. Journal of African Earth Sciences, **111:** 54–75.

Fedo, C.M., Nesbitt, H.W., Young, G.M., 1995. Unraveling the effects of potassium metasomatism in sedimentary rocks and paleosols, with implications for paleoweathering conditions and provenance. Geology, **10:** 921–924.

Gabrielli, P., Wegner, A., Petit, J.R., Delmonte, B., De Deckker, P., Gaspari, V., Fischer, H., Ruth, U., Kriews, M., Boutron, C., Cescon, P., Barbante, C., 2010. A major glacial-interglacial change in aeolian dust composition inferred from rare earth elements in Antarctic ice. Quaternary Science Reviews, **29:** 265–273.

Garver, J.I., Royce, P.R., Smick, T.A., 1996. Chromium and nickel in shale of the Taconic Foreland: a case study for the provenance of fine-grained sediments with an ultramafic source. Journal of Sedimentary Research, **66:** 100–106.

Hair, J.F., Anderson, R.E., Taham, R.L., William, C.B., 2001. Análisis Multivariante. 5a Ed. Prentice Hall: 794.

Hallberg, R.O., 1976. A geochemical method for investigation of palaeoredox conditions in sediments. Ambio Special Report, **4:** 139–147.

Harnois, L., 1988. The CIW index: a new chemical index of weathering. Sedimentary Geology, **55:** 319–322.

Hernández-Hinojosa, V., Montiel-García, P.C., Armstrong-Altrin, J.S., Nagarajan, R., Kasper-Zubillaga, J.J., 2018. Textural and geochemical characteristics of beach sands along the western Gulf of Mexico, Mexico. Carpathian Journal of Earth and Environmental Sciences, **13:** 161–174.

Herron, M.M., 1988. Geochemical classification of terrigenous sands and shales from core or log data. Journal of Sedimentary Petrology, **58:** 820–829.

Hou, Q., Mou, C., Wang, Q., Tan, Z., 2017. Provenance and tectonic setting of the Early and Middle Devonian Xueshan Formation, the North Qilian Belt, China. Geological Journal 1–19 doi: 10.1002/gj.2963

Hu, G., Hu, W-X., Cao, J., Yang, R-F., Chen, H-Y., Zhao, D-F., Pang, Q., Wang, H-Y., Tan, X-C., 2017. The distribution, hydrocarbon potential, and development of the Lower Cretaceous black shales in coastal southeastern China. Journal of Palaeogeography, **6:** 333–351.

Hua, G., Yuansheng, D., Lian, Z., Jianghai, Y., Hu, H., Min, L., Yuan, W., 2013. Trace and rare earth elemental geochemistry of carbonate succession in the Middle Gaoyuzhuang Formation, Pingquan Section: Implications for Early Mesoproterozoic Ocean redox conditions. Journal of Palaeogeography, **2:** 209–221.

Jones, B., Manning, D.C., 1994. Comparison of geochemical indices used for the interpretation of paleo-redox conditions in Ancient mudstones. Chemical Geology, **111:** 111–129.

Kasper-Zubillaga, J.J., Armstrong-Altrin, J.S., Carranza-Edwards, A., Morton-Bermea, O., Lozano-Santa-Cruz, R., 2013. Control in beach and dune sands of the Gulf of Mexico and the role of nearby rivers. International Journal of Geosciences, **4:** 1157–1174.

Kasper-Zubillaga, J.J., Arellano-Torres, E., Armstrong-Altrin, J.S., 2019. Physical degradation and early diagenesis in foraminiferal tests after subaerial exposure in terrigenous-depleted beaches of Yucatan, Mexico. Carbonates and Evaporites, doi: https://doi.org/10.1007/s13146-019-00485-4

Kelepile, T., Betsi, T.B., Franchi, F., Shemang, E., Suh, C.E., 2017. Provenance and tectonic setting of the Neoproterozoic clastic rocks hosting the Banana Zone Cu-Ag mineralisation, northwest Botswana. Journal of African Earth Sciences, **129:** 853–869.

Khan, R., Rouf, M.A., Das, S., Tamin, U., Naher, K., Podder, J., Hossain, S.M., 2017. Spatial and multi-layered assessment of heavy metals in the sand of Coxs-Bazar beach of Bangladesh. Regional Studies in Marine Science, **16:** 171–180.

Le Bas, M.J., Le Maitre, R.W., Streckeisen, A., Zanettin, B., 1986. A chemical classification of volcanic rocks based on the total alkali-silica diagram. Journal of Petrology, **27:** 745–750.

Lee, Y.I., 2009. Geochemistry of shales of the Upper Cretaceous Hayang Group, SE Korea: implications for provenance and source weathering at an active continental margin. Sedimentary Geology, **215:** 1–12.

Lin, C-M., Zhang, X., Zhang, N., Chen, S-Y, Liu, M., 2014. Provenance records of the north Jiangsu Basin, east China: zircon U-Pb geochronology and geochemistry from the Paleogene Dainan Formation in the Gaoyou Sag. Journal of Palaeogeography, **3**: 99–114.

Liu, B., Jin, H.L., Sun, L.Y., Sun, Z., Niu, Q.H., Zhang, C.X., 2016. Geochemical characteristics of Holocene aeolian deposits and their environmental significance in the Mu Us desert, northern China. Geological Journal, **51:** 325–337.

Long, E.R., Macdonald, D.D., Smith, S.L., 1995. Incidence of adverse biological effects within ranges of chemical concentrations in marine and estuarine sediments. Environmental Management, **1:** 81–97.

Ma, K., Hu, S., Wang, T., Zhang, B., Qin, S., Shi, S., Wang, K., Qingyu, H., 2017. Sedimentary environments and mechanisms of organic matter enrichment in the Mesoproterozoic Hongshuizhuang Formation of northern China. Palaeogeography, Paleoclimatology, Palaeoecology, **475:** 176–187.

Ma, M., Chen, G., Lyu, C., Zhang, G., Li, C., Yan, Y., Ma, Z., 2019. The formation and evolution of the paleo-Pearl River and its influence on the source of the northern South China Sea. Marine and Petroleum Geology, **106:** 171–189.

Madhavaraju, J., 2015. Geochemistry of Campanian-Maastrichtian sedimentary rocks in the Cauvery Basin, South India: Constrains on paleoweathering, provenance and end Cretaceous environments. Chemostratigraphy: Concepts, Techniques and Applications (ed. M. Ramkumar): 185–214. Elsevier Special Volume.

Madhavaraju, J., Lee, Y.I., 2010. Influence of Deccan Volcanism in the sedimentary rocks of Late Maastrichtian-Danian age of Cauvery Basin, Southeastern India: constraints from Geochemistry. Current Science, **98:** 528–537.

Madhavaraju, J., Tom, M., Lee, Y.I., Balaram, V., Ramasamy, S., Carranza-Edwards, A., Ramachandran, A., 2016. Provenance and tectonic settings of sands from Puerto Peñasco, Desemboque and Bahia Kino beaches, Gulf of California, Sonora, Mexico. Journal of South American Earth Sciences, **71:** 262–275.

Madhavaraju, J., Pacheco-Olivas, S.A., González-León, C.M., Espinoza-Maldonado, I.G., Sanchez-Medrano, P.A., Villanueva-Amadoz, U., Monreal, R., Pi-Puig, T., Ramírez-Montoya, E., Grijalva-Noriega, F.J., 2017. Mineralogy and geochemistry of the Lower Cretaceous siliciclastic rocks of the Morita Formation, Sierra San José section, Sonora, Mexico. Journal of South American Earth Sciences, **76:** 397–411.

Madhavaraju, J., Saucedo-Samaniego, J.C., Loser, H., Espinoza-Maldonado, I.G., Solari, L., Monreal, R., Grijalva--Noriega, F.J., Jaques-Ayala, C., 2018. Detrital zircon record of Mesozoic volcanic arcs in the Lower Cretaceous Mural Limestone, Northwestern Mexico. Geological Journal: 1–25. https://doi.org/10.1002/gj.3315

Martinez, N.C., Murray, R.W., Thunel, R.C., Peterson, L.C., Muller-Karger, F., Lorenzoni, L., Astor, Y., Varela, R., 2010. Local and regional geochemical signatures of surface sediments from the Cariaco Basin and Orinoco Delta, Venezuela. Geology, **38:** 159–162.

McLennan, S.M., Hemming, S., McDaniel, D.K., Hanson, G.N., 1993. Geochemical approaches to sedimentation, provenance, and tectonics. In: Processes Controlling the Composition of Clastic Sediments (eds. M.J. Johnsson and A. Basu): 21–40. Geological Society of America Special Paper.

Monreal-Gómez, M.A., Salas de León, D.A., 1990. Simulación de la circulación de la Bahía de Campeche. Geofísica Internacional, **29:** 101–111.

Morford, J.L., Emerson, S., 1999. The geochemistry of redox sensitive trace metals in sediments. Geochimica et Cosmochimca Acta, **63:** 1735–1750.

Müller, G., 1969. Index of geoaccumulation in sediments of the Rhine River. Geojournal, **2:** 108–118.

Müller, G., 1979. Schwermetalle in den sedimenten des Rheins--Veranderungen seitt 1971. Umschan, **79:** 778–783.

Murray, R.W., Leinen, M., 1996. Scavenged excess aluminum and its relationship to bulk titanium in biogenic sediment from the central equatorial Pacific Ocean. Geochimica et Cosmochimica Acta, **60:** 3869–3878.

Nagarajan, R., Armstrong-Altrin, J.S., Kessler, F.L., Hidalgo--Moral, E.L., Dodge-Wan, D., Taib, N.I., 2015. Provenance and tectonic setting of Miocene siliciclastic sediments, Sibuti formation, northwestern Borneo. Arabian Journal of Geosciences, **8:** 8549–8565.

Nagarajan, R., Armstrong-Altrin, J.S., Kessler, F.L., Jong, J., 2017. Petrological and geochemical constraints on provenance, paleo-weathering and tectonic setting of clastic sediments from the Neogene Lambir and Sibuti Formations, Northwestern Borneo. In: Sediment Provenanc (ed. Rajat Mazumder): 123–153 e. Elsevier Amsterdam, Netherlands. Chapter 7. doi:10.1016/B978-0-12-803386-9.00007-1

Ndjigui, P-D., Bayiga, E.C., Onana, V.L., Djenabou-Fadil, S., Ngono, G.S.A., 2019. Mineralogy and geochemistry of recent alluvial sediments from the Ngaye River watershed, northern Cameroon: implications for the surface processes and Au-PGE distribution. Journal of African Earth Sciences, **150:** 136–157.

Nesbitt, H.W., Young, G.M., 1982. Early Proterozoic climate and plate motions inferred from major element chemistry of lutites. Nature, **299:** 715–717.

Nesbitt, H.W., Fedo, C.M., Young, G.M., 1997. Quartz and feldspar stability, steady and non-steady-state weathering, and petrogenesis of siliciclastic sands and muds. Journal of Geology, **105:** 173–192.

Ortega-Gutierrez, F., Ruiz, J., Centeno-García, E., 1995. Oaxaquia, a Proterozoic microcontinent accreted to North America during the late Paleozoic. Geology, **23:** 1127–1130.

Ouyang, Y., 2005. Evaluation of river water quality monitoring stations by principal component analysis. Water Research, **39:** 2621–2635.

Paikaray, S., Banerjee, S., Mukherji, S., 2008. Geochemistry of shales from the Paleoproterozoic to Neoproterozoic Vindhyan Supergroup: implications on provenance, tectonics and paleoweathering. Journal of Asian Earth Sciences, **32:** 34–48.

Pandey, S., Parcha, S.K., 2017. Provenance, tectonic setting and source-area weathering of the lower Cambrian sediments of the Parahio valley in the Spiti basin, India. Journal of Earth System Science, **126**: 27.

Parker, A., 1970. An index of weathering for silicate rocks. Geological Magazine, **107:** 501–504.

Prabakaran, K., Nagarajan, R., Eswaramoorthi, S., Anandkumar, A., Franco, F.M., 2019. Environmental significance and geochemical speciation of trace elements in Lower Baram River sediments. Chemosphere, **219:** 933–953.

Price, J.R., Velbel, M.A., 2003. Chemical weathering indices applied to weathering profiles developed on heterogeneous felsic metamorphic parent rocks. Chemical Geology, **202:** 397–416.

Qiu, S., Zhu, Z., Yang, T., Wu, Y., Bai, Y., Ouyang, T., 2014. Chemical weathering of monsoonal eastern China: implications from major elements of topsoil. Journal of Asian Earth Sciences, **81:** 77–90.

Ramachandran, A., Madhavaraju, J., Ramasamy, S., Lee, Y.I., Rao, S., Chawngthu, D.L., Velmurugan, K., 2016. Geochemistry of Proterozoic clastic rocks of the Kerur Formation of Kaladgi-Badami Basin, North Karnataka, South India: implications for paleoweathering and provenance. Turkish Journal of Earth Sciences, **25:** 126–144.

Ramos-Vázquez, M., Armstrong-Altrin, J.S., Rosales-Hoz, L., Machain-Castillo, M.L., and Carranza-Edwards, A., 2017. Geochemistry of deep-sea sediments in two cores retrieved at the mouth of the Coatzacoalcos river delta, Western Gulf of Mexico, Mexico. Arabian Journal of Geosciences, **10:** 148.

Ramos-Vázquez, M.A., Armstrong-Altrin, J.S., Machain--Castillo, M.L., Gío-Argáez, F.R. 2018. Foraminiferal assemblages, ^{14}C ages, and compositional variations in two sediment cores in the western Gulf of Mexico. Journal of South American Earth Sciences, **88:** 480–496.

Riquier, L., Tribovillard, N., Averbuch, O., Devleeschouwer, X., Riboulleau, A., 2006. The late Frasnian Kellwasser horizons of the Harz Mountains (Germany): two oxygen-deficient periods resulting from different mechanisms. Chemical Geology, **233:** 137–155.

Rosales-Hoz, L., Carranza-Edwards, A., Martínez-Serrano, R., Alatorre, M.A, Armstrong-Altrin, J.S., 2015. Textural and geochemical characteristics of marine sediments in the SW Gulf of Mexico: implications for source and seasonal change. Environmental Monitoring and Assessment, **187–205:** 1–19.

Roser, B.P., Korsch, R.J., 1988. Provenance signatures of sandstone–mudstone suites determined using discrimination function analysis of major-element data. Chemical Geology, **67:** 119–139.

Salas de León, D.A., Monreal-Gomez, M.A., Colunga-Enríquez, G., 1992. Hidrografía y circulación geostrófica en el sur de la Bahía de Campeche. Geofísica Internacional, **31:** 315–323.

Salas-Monreal, D., Marin-Hernandez, M., Salas-Perez, J.J., Salas-de-Leon, D.A., Monreal-Gomez, M.A., Perez-España, H., 2018. Coral reef connectivity within the Western Gulf of Mexico. Journal of Marine Systems, **179:** 88–99.

Schaaf, P., Stimac, J., Siebe, C., Macías, J.L., 2005. Geochemical evidence for mantle origin and crustal processes in volcanic rocks from Popocatépetl and surrounding monogenetic volcanoes, Central Mexico. Journal of Petrology, **46:** 1243–1282.

Selvaraj, K., Ram, V., Szefer, P., 2004. Evaluation of metal contamination in coastal sediments Bay of Bengal, India: geochemical and statistical approaches. Marine Pollution Bulletin, **49:** 174–185.

Shaw, T.J., Geiskes, J.M., Jahnke, R.A., 1990. Early diagenesis in differing depositional environments: the response of transition metals in pore water. Geochimica et Cosmochimica Acta, **54:** 1233–1246.

Shepard, F.P., 1954. Nomenclature based on sand-silt-clay ratios. Journal of Sedimentary Petrology, **24:** 151–158.

Spalletti, L.A., Remírez, M.N., Sagasti, G., 2019. Geochemistry of aggradational – progradational sequence sets of the Upper Jurassic – Lower Cretaceous Vaca Muerta shales (Añelo area, Neuquén Basin, Argentina): Relation to changes in accommodation and marine anoxia. Journal of South American Earth Sciences, https://doi.org/10.1016/ j.jsames.2019.02.011

Taheri, A., Jafarzadeh, M., Armstrong-Altrin, J.S., Mirbagheri, S.R., 2018. Geochemistry of siliciclastic rocks from the Shemshak Group (Upper Triassic-Lower-Middle Jurassic), northeastern Alborz, northern Iran: implications for palaeoweathering, provenance, and tectonic setting. Geological Quarterly, **62** (3)**:** 522–535.

Tamayo, J.L., 1991. Geografía Moderna de México, 11th ed. Trillas, México City.

Tapia-Fernandez, H.J., Armstrong-Altrin, J.S., Selvaraj, K., 2017. Geochemistry and U-Pb geochronology of detrital zircons in the Brujas beach sands, Campeche, Southwestern Gulf of Mexico, Mexico. Journal of South American Earth Sciences, **76:** 346–361.

Tawfik, H.A., Ghandour, I.M., Maejima, W., Armstrong-Altrin, J.S., Abdel-Hameed, A-M.T., 2017. Petrography and geochemistry of the siliciclastic Araba Formation (Cambrian), east Sinai, Egypt: Implications for provenance, tectonic setting and source weathering. Geological Magazine, **154:** 1–23.

Tawfik, H.A., Salah, M.K., Maejima, W., Armstrong-Altrin, J.S., Abdel-Hameed, A-M.T., Ghandour, M.M.E., 2018. Petrography and geochemistry of the Lower Miocene Moghra sandstones, Qattara Depression, north Western Desert, Egypt. Geological Journal, **53**: 1938–1953.

Taylor, S.R., McLennan, S.M., 1985. The Continental Crust: its Composition and Evolution. Oxford, UK. Blackwell.

Tzifas, I.T., Papadopoulos, A., Misaelides, P., Godelitsas, A., GŘttlicher, J., Tsikos, H., Gamaletsos, P.N., Luvizotto, G., Karydas, A.G., Petrelli, M., Noli, F., Kantarelou, V., Kontofakas, A., Hatzidimitriou, A., 2019. New insights into mineralogy and geochemistry of allanite-bearing Mediterranean coastal sands from Northern Greece. Geochemistry, **79**: 247–267.

Velmurugan, K., Madhavaraju, J., Balaram, V., Ramasamy, S., Ramachandran, A., Ramirez-Montoya, E., Saucedo-Samaniego, J.C., 2019. Provenance and tectonic setting of the clastic rocks of the Kerur Formation, Badami Group, Mohare area, Karnataka, India. In: Precambrian Crustal Evolution of India: Geological Evolution of the Precambrian Indian Shield (ed. M.E.A. Mondal): 239–269. Society of Earth Scientist Series by Springer-Verlag, 1st Edition.

Verma, S.P., 1999. Geochemistry of evolved magmas and their relationship to subduction-unrelated mafic volcanism at the volcanic front of the central Mexican Volcanic Belt. Journal of Volcanology and Geothermal Research, **93:** 151–171.

Verma, S.P., 2000. Geochemical evidence for a lithospheric source for magmas from Los Humeros caldera, Puebla, Mexico. Chemical Geology, **164:** 35–60.

Verma, S.P., 2001a. Geochemical evidence for a Rift-Related Origin of bimodal volcanism at Meseta Río San Juan, North-Central Mexican Volcanic Belt. International Geology, Review, **43:** 475–493.

Verma, S.P., 2001b. Geochemical evidence for a lithospheric source for magmas from Acoculco Caldera, Eastern Mexican Volcanic Belt. International Geology Review, **43:** 31–51.

Verma, S.P., 2005. Estadística Básica para el Manejo de Datos Experimentales: Aplicación a la Geoquímica (Geoquimiometría) (in Spanish). Universidad Nacional Autónoma de México, México, D.F.

Verma, S.P., 2015. Origin, evolution, and tectonic setting of the eastern part of the Mexican Volcanic Belt and comparison with the Central American Volcanic Arc from conventional multielement normalized and new multidimensional discrimination diagrams and discordancy and significance tests. Turkish Journal of Earth Sciences, **24:** 111–164.

Verma, S.P., Armstrong-Altrin, J.S., 2013. New multi-dimensional diagrams for tectonic discrimination of siliciclastic sediments and their application to Precambrian basins. Chemical Geology, **355:** 117–180.

Verma, S.P., Armstrong-Altrin, J.S., 2016. Geochemical discrimination of siliciclastic sediments from active and passive margin settings. Sedimentary Geology, **332:** 1–12.

Verma, S.P., Díaz-González, L., Armstrong-Altrin, J.S., 2016. Application of a new computer program for tectonic discrimination of Cambrian to Holocene clastic sediments. Earth Science Informatics, **9:** 151–165.

Wang, Z., Wang, J., Fu, X., Zhan, W., Yu, F., Feng, X., Song, C., Chen, W., Zeng, S., 2017. Organic material accumulation of Carnian mudstones in the North Qiangtang Depression, eastern Tethys: controlled by the paleoclimate, paleoenvironment, and provenance. Marine and Petroleum Geology, **88:** 44–457.

Wang, Z., Wang, J., Fu, X., Zhan, W., Armstrong-Altrin, J.S., Yu, F., Feng, X., Song, C., Zeng, S., 2018. Geochemistry of the Upper Triassic black mudstones in the Qiangtang Basin, Tibet: implications for paleoenvironment, provenance, and tectonic setting. Journal of Asian Earth Sciences, **160:** 118–135.

Wedepohl, H.K., 1995. The composition of the continental crust. Geochimica et Cosmochimica Acta, **59:** 1217–1232.

Xie, Y., Chi, Y., 2016. Geochemical investigation of dry- and wet-deposited dust during the same dust-storm event in Harbin, China: constraint on provenance and implications for formation of aeolian loess. Journal of Asian Earth Sciences, **120:** 43–61.

Yang, J-H., Du, Y-S., 2017. Weathering geochemistry and palaeoclimate implication of the Early Permian mudstones from eastern Henan Province, North China. Journal of Palaeogeography, **6:** 370–380.

Yañez-Arancibia, A., Day, J.W. Jr., 1982. Ecological characterization of Terminos Lagoon: a tropical lagoon estuarine system in the southern Gulf of Mexico. Oceanologica Acta, **5:** 431–500.

Zaid, S.M., 2013. Provenance, diagenesis, tectonic setting and reservoir quality of the sandstones of the Kareem Formation, Gulf of Suez, Egypt. Journal of African Earth Sciences, **85:** 31–52.

Zaid, S.M., 2017. Provenance of coastal dune sands along Red Sea, Egypt. Journal of Earth System Science, **126:** 50.

Zaid, S.M., Gahtani, F.A., 2015. Provenance, diagenesis, tectonic setting and geochemistry of Hawkesbury sandstone (Middle Triassic), southern Sydney Basin, Australia. Turkish Journal of Earth Sciences, **24:** 72–98.

Zhang, S., Hu, Z., Wang, H., 2018. A retrospective review of microbiological methods applied in studies following the deep-water horizon oil spill. Frontiers in Microbiology, **9:** 520.